

# Detecting the weak high-frequency character signal by vibrational resonance in the Duffing oscillator

H. G. Liu  · X. L. Liu · J. H. Yang · Miguel A. F. Sanjuán · G. Cheng

Received: 22 February 2016 / Accepted: 8 June 2017  
© Springer Science+Business Media B.V. 2017

**Abstract** The weak high-frequency character signal (HCS) cannot be detected substantially by the traditional vibrational resonance (VR) theory. In this paper, by introducing the scale transformation, the HCS in the original system can be transformed to the low-frequency character signal in the rescaled system. As we know, the two systems are equivalent and the VR can occur at low frequency in the rescaled system. Then, the VR can also occur at high frequency in the original system. We take the underdamped bistable system and the overdamped bistable system of the Duffing oscillator as examples. The method proposed in this paper is verified by both theoretical analysis and numerical

simulations. The results obtained by the two ways are in good agreement. The results in this paper provide a tool to detect the weak character signal with arbitrary frequency in the engineering problems.

**Keywords** Weak high-frequency character signal · Scale transformation · Vibrational resonance

## 1 Introduction

Vibrational resonance (VR) is a phenomenon showing the amplification of a weak low-frequency character signal (LCS) by a high-frequency auxiliary signal (HAS) [1]. It shows many similarities to the well-known phenomenon of stochastic resonance (SR) [2–4], though the HAS replaces the noise. The noise is random, but the HAS is deterministic. So that, compared with the SR, the VR is much easier to be controlled [5]. For this reason, the VR has attracted much attention in the past few years. For example, Chizhevsky and Giacomelli have investigated the effect of the additive noise on the VR in a bistable, vertical cavity laser [6–8]. They have found that the additive noise induces a gain degradation. And compared with the SR, they have found that the VR generates a higher signal-to-noise ratio (SNR). Deng et al. have investigated the VR in neuron populations with different forms [9–11]. They have found that the optimal amplitude depends on the connection among the neurons. Yang et al. [12–14] have studied the VR

We acknowledge financial supports by the Fundamental Research Funds for the Central Universities (Grant No. 2015XKMS023), the Priority Academic Program Development of Jiangsu Higher Education Institutions, Top-notch Academic Programs Project of Jiangsu Higher Education Institutions, and the Spanish Ministry of Economy and Competitiveness (Grant No. FIS2013-40653-P).

H. G. Liu (✉) · X. L. Liu · J. H. Yang · G. Cheng  
School of Mechatronic Engineering, China University of Mining and Technology, Xuzhou 221116, China  
e-mail: liuhg@cumt.edu.cn

H. G. Liu · X. L. Liu  
Jiangsu Key Laboratory of Mine Mechanical and Electrical Equipment, China University of Mining and Technology, Xuzhou 221116, China

M. A. F. Sanjuán  
Nonlinear Dynamics, Chaos and Complex Systems Group, Departamento de Física, Universidad Rey Juan Carlos, Tulipán s/n, 28933 Móstoles, Madrid, Spain

in a fractional-order system, and they have found that the fractional-order damping influences the resonance pattern. It provides another way for us to control the weak low-frequency periodical signals in nonlinear systems. Wang et al. made investigations on VR in some other systems such as bistable gene transcriptional regulatory system [15], excitable system [16] and discrete neuron system [17]. They all showed good performance. Jeevarathinam et al. [18] applied the VR to the groundwater-dependent plant ecosystems. The study presents a new way for us to enhance the biomass response. Meanwhile, they have investigated the effect of multiple time-delay on the VR [19]. Daza et al. [20] studied the VR phenomenon in a simple time-delayed genetic toggle switch. And they found that the delay of the toggle switch affects the resonance strongly since it can also induce autonomous oscillations. Coccolo et al. [21] have shown that more energy can be harvested by using the VR phenomenon. And the new way is highly controllable. Yang et al. [22] proposed the vibrational subharmonic and superharmonic resonances. They show that the resonance happens at a frequency which is not an integer multiple of the low-frequency of the excitations.

The former researchers have carried out a lot of investigations on the VR. However, to our knowledge, almost all works on the VR were focused on the weak LCS that the frequency of the character information is usually smaller than 1 rad/s. According to the frequency response characteristic of the vibration system, we can know that the system response amplitude will become very small when the excitation frequency is away from the natural frequency of the equivalent system [23]. Meanwhile, the natural frequency of the conventional system is usually low. So, like the classic SR, the traditional VR can deal with the LCS only. However, in the engineering background, such as in the mechanical fault diagnosis field, the weak fault feature frequency usually lies in several to thousands rad/s or Hz. Based on the traditional VR theory, this kind of weak high-frequency character signal (HCS) cannot be detected. Hence, it is hard to apply the VR in engineering problems. So, our main motivation lies at solving the problem of how to extend the engineering applications of the VR.

In the SR mechanism, we have known that the techniques such as the frequency-shifted and rescaling method [24], the scale transformation method [25], the step-varying method [26], among others, can help

us to detect the weak HCS. In this paper, the scale transformation method is introduced in the study of the VR. The paper is organized as follows. In Sect. 2, by introducing the scale transformation method, we investigate the VR at high frequency in the underdamped Duffing oscillator. Similarly, we investigate the case of the overdamped Duffing oscillator in Sect. 3. Finally, the main results of this paper are briefly described in the conclusions section.

## 2 Underdamped Duffing oscillator

### 2.1 Theoretical formulation

Here, we investigate the VR at high frequency in the underdamped bistable system. The normal form of the governing equation is written as

$$\frac{d^2x}{dt^2} + 2\delta \frac{dx}{dt} = ax - bx^3 + A \cos(2\pi ft) + B \cos(2\pi Ft), \quad (1)$$

where  $A \cos(2\pi ft)$  is the weak HCS which indicates the character information and  $B \cos(2\pi Ft)$  is the HAS which is used to detect the weak character information,  $f \gg 1$  Hz,  $F \gg f$ .  $A$  and  $B$  are the amplitude of the weak HCS and the HAS, respectively.  $f$  and  $F$  are the frequency of the weak HCS and the HAS, respectively.  $\delta$  is the damping coefficient, and  $a$  and  $b$  are positive real parameters.

In order to overcome the problem that the traditional VR cannot detect the weak HCS, the scale transformation method is introduced in the following. By a scale transformation, making  $x(t) = z(\tau)$  and  $\tau = ct$ , where  $c$  is the rescaling factor, substituting  $x(t) = z(\tau)$  and  $\tau = ct$  into Eq. (1), one obtains

$$\begin{aligned} \frac{d^2z}{d\tau^2} + 2\delta \frac{1}{c} \frac{dz}{d\tau} &= \frac{a}{c^2} z - \frac{b}{c^2} z^3 + \frac{1}{c^2} A \cos\left(2\pi \frac{f}{c} \tau\right) \\ &+ \frac{1}{c^2} B \cos\left(2\pi \frac{F}{c} \tau\right) \end{aligned} \quad (2)$$

Through the scale transformation, the system parameters and the excited signals in the rescaled system are transformed compared with the original system. As described in the previous reference [27], to well realize the VR, three steps are needed to be carried out. Firstly, the amplitudes of the two signals have been decreased to  $\frac{1}{c^2}$ , so we make  $A$  and  $B$  to be multiplied by  $c^2$ . Secondly,  $\delta$  has been decreased to  $\frac{1}{c}$ , so we make  $\delta$  to be

multiplied by  $c$ . Thirdly, to normalize Eq. (2), we make the parameters  $a = b = c^2$ . Then, one obtains

$$\frac{d^2z}{d\tau^2} + 2\delta \frac{dz}{d\tau} = z - z^3 + A \cos\left(2\pi \frac{f}{c} \tau\right) + B \cos\left(2\pi \frac{F}{c} \tau\right). \tag{3}$$

According to the method of direct separation of slow and fast motions [28, 29], we know that an approximate solution of Eq. (3) is written in the form  $z = M + N$ , where  $M$  denotes the slow motion with period  $c/f$  and  $N$  denotes the fast motion with period  $c/F$ . Substituting  $z = M + N$  into Eq. (3), one obtains

$$\frac{d^2M}{d\tau^2} + \frac{d^2N}{d\tau^2} + 2\delta \frac{dM}{d\tau} + 2\delta \frac{dN}{d\tau} = M + N - M^3 - 3M^2N - 3MN^2 - N^3 + A \cos\left(2\pi \frac{f}{c} \tau\right) + B \cos\left(2\pi \frac{F}{c} \tau\right). \tag{4}$$

Searching the approximate solution of the fast motion  $N$  in the following linear equation

$$\frac{d^2N}{d\tau^2} = N + 2\delta \frac{dN}{d\tau} + B \cos\left(2\pi \frac{F}{c} \tau\right), \tag{5}$$

then substituting the approximate solution  $N = A_H \cos(2\pi F\tau/c + \psi)$  into Eq. (5), one gets

$$A_H = \frac{B}{\sqrt{\left(2\pi \frac{F}{c} 2\pi \frac{F}{c} + 1\right)^2 + \left(2\delta 2\pi \frac{F}{c}\right)^2}}. \tag{6}$$

Further, substituting the approximate solution  $N = A_H \cos(2\pi F\tau/c + \psi)$  into Eq. (4) and averaging all terms in the interval  $[0, c/F]$ , one obtains the slow motion  $M$  that is governed by

$$\frac{d^2M}{d\tau^2} + 2\delta \frac{dM}{d\tau} = \left(1 - \frac{3}{2}A_H^2\right)M - M^3 + A \cos\left(2\pi \frac{f}{c} \tau\right) \tag{7}$$

From Eq. (7), one obtains the stable equilibrium points  $M^*$ . When  $(1 - 3A_H^2/2) > 0$ ,  $M^* = \pm \sqrt{\left(1 - \frac{3A_H^2}{2}\right)}$ ; when  $(1 - 3A_H^2/2) < 0$ ,  $M^* = 0$ . Considering the deviation  $Y$  of  $M$  from  $M^*$ , substituting  $Y = M - M^*$  into Eq. (7). There are two cases:

Firstly,  $(1 - 3A_H^2/2) > 0$  and  $M^* = \pm \sqrt{\left(1 - \frac{3A_H^2}{2}\right)}$ , substituting  $Y = M - M^*$  into Eq. (7). To obtain the

response at the frequency  $f/c$ , one should solve the following linear equation

$$\frac{d^2Y}{d\tau^2} + 2\delta \frac{dY}{d\tau} = \left(3A_H^2 - 2\right)Y + A \cos\left(2\pi \frac{f}{c} \tau\right) \tag{8}$$

Substituting the approximate solution  $Y = A_L \cos(2\pi f\tau/c + \theta)$  into Eq. (8), it is easy to obtain

$$A_L = \frac{A}{\sqrt{\left(2\pi \frac{f}{c} 2\pi \frac{f}{c} + 3A_H^2 - 2\right)^2 + \left(2\delta 2\pi \frac{f}{c}\right)^2}}. \tag{9}$$

To evaluate the effect of the VR, the amplification factor  $Q$  is treated as a measurement in this paper, which is defined by  $Q = A_L/A$ . Taking into account Eq. (9), one obtains

$$Q = \frac{A_L}{A} = \frac{1}{\sqrt{\left(2\pi \frac{f}{c} 2\pi \frac{f}{c} + 3A_H^2 - 2\right)^2 + \left(2\delta 2\pi \frac{f}{c}\right)^2}}. \tag{10}$$

Secondly,  $(1 - 3A_H^2/2) < 0$  and  $M^* = 0$ . The amplification factor  $Q$  is described by

$$Q = \frac{A_L}{A} = \frac{1}{\sqrt{\left(2\pi \frac{f}{c} 2\pi \frac{f}{c} + \left(1 - \frac{3A_H^2}{2}\right)\right)^2 + \left(2\delta 2\pi \frac{f}{c}\right)^2}}. \tag{11}$$

The VR at a high frequency can be discussed by the theoretical prediction in Eqs. (10) and (11).

### 2.2 Numerical simulations

In order to verify the accuracy of the theoretical formulation, numerical simulations are carried out in this section. In our numerical simulations, the response amplitude  $W(f_i)$  is defined as follows [22]

$$\begin{cases} W_s(f_i) = \frac{2}{rT} \int_0^{rT} x(t) \sin(2\pi f_i t) dt \\ W_c(f_i) = \frac{2}{rT} \int_0^{rT} x(t) \cos(2\pi f_i t) dt \\ W(f_i) = \sqrt{W_s^2(f_i) + W_c^2(f_i)} \end{cases} \tag{12}$$

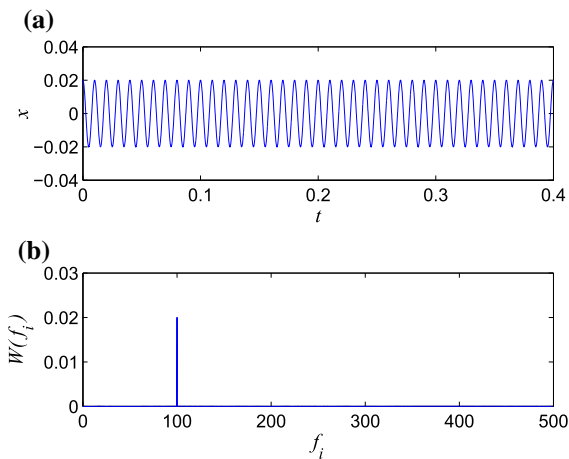


**Fig. 1** **a** The time series of the weak HCS; **b** the amplitude spectrum of the response. The simulation parameters are  $A = 0.02$  and  $f = 100$

where  $W_s(f_i)$  and  $W_c(f_i)$  are the sine and cosine Fourier components of the output at the arbitrary frequency  $f_i$ . Here,  $f_i$  means all potential frequencies that may be included in the output. It is because some other frequency components besides the excitation frequencies are included in the response according to the nonlinear response theory [28]. Through Eq. (12), we can obtain the amplitude spectrum of the response. The period  $T = 1/f$  and  $r$  is a large enough integer number. Then, the amplification factor  $Q$  at the excitation low frequency  $f$  can be described by  $Q = W(f)/A$ . The time series of the weak HCS is shown in Fig. 1. It is a simple cosine signal with the simulation parameters  $f = 100\text{Hz}$  and the  $A = 0.02$ .

Then, the weak HCS will be detected by the VR in the rescaled system. In the rescaled system, the frequency of the HAS is 1500 Hz. The damping coefficient  $\delta$  is 0.1. The variable  $B$  increases from 0 to 140. The rescaling factor  $c$  is set as 1000. Figure 2 shows that the curve of the amplification factor  $Q$  versus the amplitude of the HAS presents VR. The curve shows an apparent double-resonance pattern. Meanwhile, the numerical and the theoretical results are in close agreement. In the curve of the numerical simulation, the maximum amplification factor  $Q$  is 7.695 and the corresponding amplitude  $B$  is 88. When  $B$  is set to 88, the system output curve is shown in Fig. 3. Figure 3 shows that the VR phenomenon is visible compared with Fig. 1.

In order to investigate the influence of the amplitude and the frequency of the weak HCS on the VR, we plot

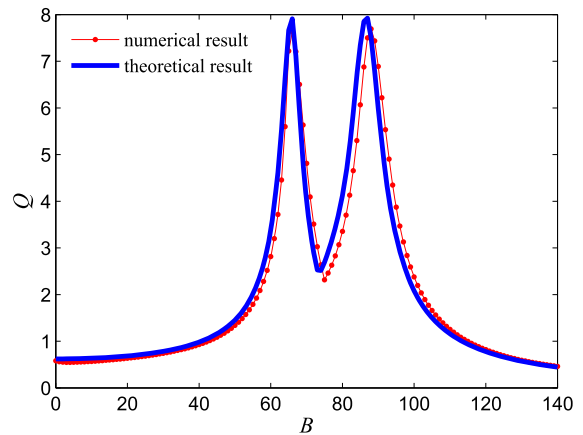


**Fig. 2** Amplification factor  $Q$  versus the amplitude of the HAS. The *thick line* is the theoretical result, while the *thin line with markers* is the numerical result. The simulation parameters are  $c = 1000$ ,  $a = b = 10^6$ ,  $A = 0.02$ ,  $f = 100$ ,  $F = 1500$  and  $\delta = 0.1$

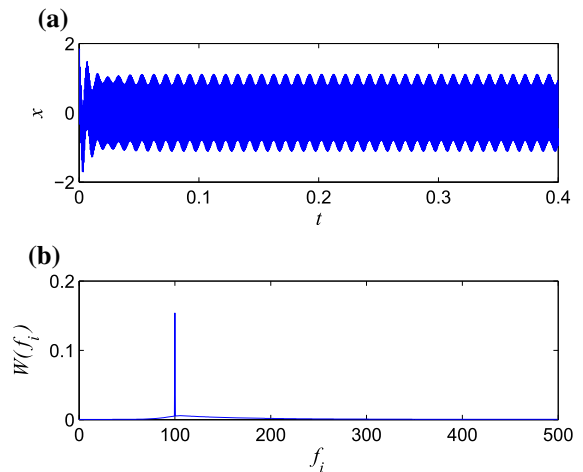


**Fig. 3** Output of the system when the VR occurs. **a** The time series of the output; **b** the amplitude spectrum of the response. The simulation parameters are  $c = 1000$ ,  $a = b = 10^6$ ,  $A = 0.02$ ,  $B = 88$ ,  $f = 100$ ,  $F = 1500$  and  $\delta = 0.1$

the curves that is the amplification factor  $Q$  versus the amplitude of the HAS for different values of  $A$  and  $f$ . The curves including numerical and theoretical results are shown in Figs. 4 and 5.

Figure 4 shows that the curves of the theoretical results do not change with the increase of  $A$ . This fact can also be verified from Eqs. (10) and (11) that the amplification factor  $Q$  has nothing to do with  $A$ . But for the numerical results, with the increase of  $A$ , the first resonance peak value decreases. And the curve of

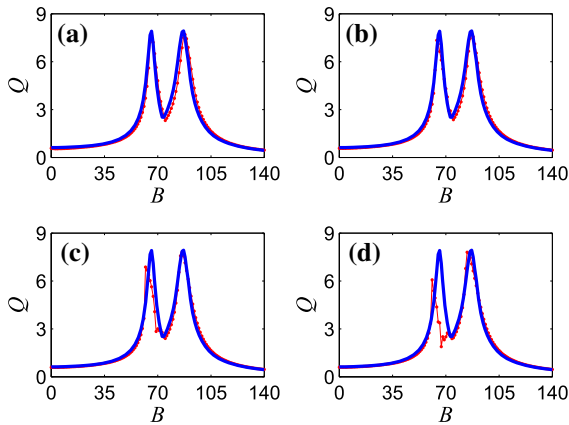


**Fig. 4** Amplification factor  $Q$  versus the amplitude of the HAS for **a**  $A = 0.02$ , **b**  $A = 0.03$ , **c**  $A = 0.04$ , **d**  $A = 0.05$ . The bold lines are the theoretical results, while the light lines with markers are the numerical results. The simulation parameters are  $c = 1000$ ,  $a = b = 10^6$ ,  $f = 100$ ,  $F = 1500$  and  $\delta = 0.1$

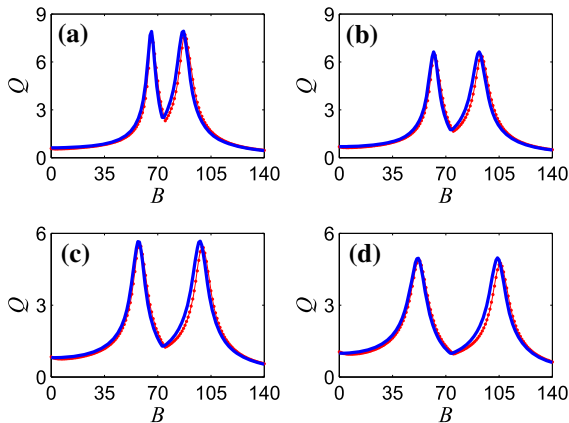


**Fig. 5** Amplification factor  $Q$  versus the amplitude of the HAS for **a**  $f = 100$ ; **b**  $f = 120$ ; **c**  $f = 140$ ; **d**  $f = 160$ . The thick lines are the theoretical results, while the thin lines with markers are the numerical results. The simulation parameters are  $c = 1000$ ,  $a = b = 10^6$ ,  $A = 0.02$ ,  $F = 1500$  and  $\delta = 0.1$

the numerical simulation is away from the curve of the theoretical formulation. This is because the method of the direct partition of slow and fast motions is sensitive to the excitations [30].

Figure 5 shows that with the increase of  $f$ , the amplification factor  $Q$  decreases in the numerical and theoretical curves. This fact can also be verified from Eq. (10) or Eq. (11). Because the amplification factor  $Q$  is a decreasing function of the variable  $f$ . In this figure, the numerical and theoretical results are in close agreement, independently of the value of  $f$ .

From Figs. 1, 2, 3, 4 and 5, we conclude that by introducing the scale transformation, the VR in the underdamped Duffing oscillator is excellent in detecting the weak HCS.

### 3 Overdamped Duffing oscillator

#### 3.1 Theoretical formulation

In this section, we investigate the VR at high frequency in the overdamped bistable system. The governing equation of the overdamped Duffing oscillator excited by two high-frequency signals is described by

$$\frac{dx}{dt} = ax - bx^3 + A \cos(2\pi ft) + B \cos(2\pi Ft). \quad (13)$$

As in Sect. 2.1, the scale transformation is still used in this section. Here, making  $x(t) = z(\tau)$  and  $\tau = ct$ . Substituting  $x(t) = z(\tau)$  and  $\tau = ct$  into Eq. (13), one obtains

$$\begin{aligned} \frac{dz}{d\tau} &= \frac{a}{c}z - \frac{b}{c}z^3 + \frac{1}{c}A \cos\left(2\pi \frac{f}{c}\tau\right) \\ &+ \frac{1}{c}B \cos\left(2\pi \frac{F}{c}\tau\right). \end{aligned} \quad (14)$$

Through the scale transformation,  $a$ ,  $b$ ,  $A$  and  $B$  are changed compared with the original. However, different from Sect. 2.1, only two steps are needed to be carried out. Firstly, making  $A$  and  $B$  multiplied by  $c$ . Secondly, making  $a = b = c$ . Then, one obtains

$$\frac{dz}{d\tau} = z - z^3 + A \cos\left(2\pi \frac{f}{c}\tau\right) + B \cos\left(2\pi \frac{F}{c}\tau\right). \quad (15)$$

Then, substituting  $z = M + N$  into Eq. (15), one obtains

$$\begin{aligned} \frac{dM}{d\tau} + \frac{dN}{d\tau} &= M + N - M^3 - 3M^2N - 3MN^2 - N^3 \\ &+ A \cos\left(2\pi \frac{f}{c}\tau\right) + B \cos\left(2\pi \frac{F}{c}\tau\right). \end{aligned} \quad (16)$$

Searching the approximate of the fast motion  $N$  in the following linear equation

$$\frac{dN}{d\tau} = N + B \cos\left(2\pi \frac{F}{c}\tau\right) \quad (17)$$

and substituting the approximate solution  $N = A_H \cos(2\pi F \tau + \psi)$  into Eq. (17), one obtains

$$A_H = \frac{B}{\sqrt{1 + (2\pi \frac{F}{c})^2}}. \tag{18}$$

Then, substituting the approximate solution  $N = A_H \cos(2\pi F \tau/c + \psi)$  into Eq. (16) and averaging all terms in the interval  $[0, c/F]$ , one obtains the slow motion  $M$  that is governed by

$$\frac{dM}{d\tau} = \left(1 - \frac{3}{2}A_H^2\right)M - M^3 + A \cos\left(2\pi \frac{f}{c} \tau\right). \tag{19}$$

From Eq. (19), one can obtain the stable equilibrium points  $M^*$ . When  $(1 - 3A_H^2/2) > 0$ ,  $M^* = \pm \sqrt{(1 - \frac{3A_H^2}{2})}$ ; when  $(1 - 3A_H^2/2) < 0$ ,  $M^* = 0$ . Considering the deviation  $Y$  of  $M$  from  $M^*$ , substituting  $Y = M - M^*$  into Eq. (19).

Firstly,  $(1 - 3A_H^2/2) > 0$  and  $M^* = \pm \sqrt{(1 - \frac{3A_H^2}{2})}$ , substituting  $Y = M - M^*$  into Eq. (19). Just considering the response at the frequency  $f/c$ , one obtains

$$\frac{dY}{d\tau} = (3A_H^2 - 2)Y + A \cos\left(2\pi \frac{f}{c} \tau\right). \tag{20}$$

Now, substituting the approximate solution  $Y = A_L \cos(2\pi f \tau/c + \theta)$  into Eq. (20), we get

$$A_L = \frac{A}{\sqrt{(3A_H^2 - 2)^2 + (2\pi \frac{f}{c})^2}}. \tag{21}$$

From Eq. (21), one obtains the amplification factor  $Q$

$$Q = \frac{A_L}{A} = \frac{1}{\sqrt{(3A_H^2 - 2)^2 + (2\pi \frac{f}{c})^2}}. \tag{22}$$

Secondly,  $(1 - 3A_H^2/2) < 0$  and  $M^* = 0$ . The amplification factor  $Q$  is

$$Q = \frac{A_L}{A} = \frac{1}{\sqrt{(1 - 3\frac{A_H^2}{2})^2 + (2\pi \frac{f}{c})^2}}. \tag{23}$$

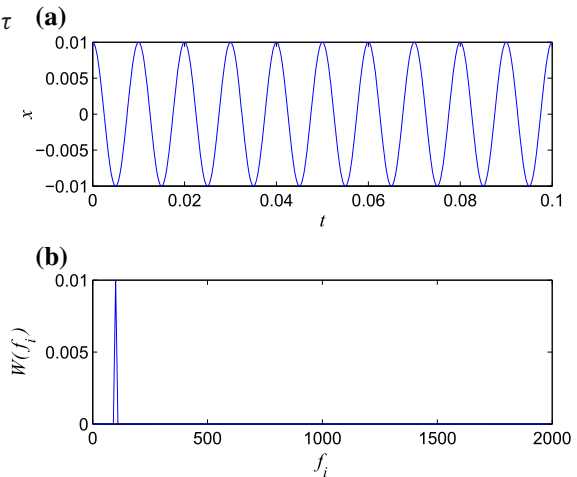


**Fig. 6** **a** The time series of the weak HCS; **b** the amplitude spectrum of the response. The simulation parameters are  $A = 0.01$  and  $f = 100$ .

### 3.2 Numerical simulations

Similarly to the Sect. 2.2, the weak HCS in this section is shown in Fig. 6. It is a simple cosine signal with the simulation parameters  $f = 100$  Hz and  $A = 0.01$ .

Then, the weak HCS is an input to the rescaled system. In the rescaled system, the frequency of the HAS is 4000 Hz. The control parameter  $B$  varies from 0 to 4. The rescaling factor  $c$  is set as 10,000. In Fig. 7, the amplification factor  $Q$  versus the amplitude of the HAS presents a single-resonance pattern. It is different from the underdamped system. Meanwhile, the numerical and theoretical results are in good agreement. In the curve of the numerical simulation, the maximum amplification factor  $Q$  is 15.45 and the corresponding amplitude  $B$  is 2.1. When  $B$  is set to 2.1, the system output curve is shown in Fig. 8. Similarly as in Fig. 3, the VR phenomenon in Fig. 8 apparently occurs.

In Fig. 9, the amplification factor  $Q$  versus the amplitude of the high-frequency auxiliary signal is given for different values of  $A$ . In this figure, the theoretical result does not change with the increase of  $A$ . This fact can also be verified from Eq. (22) or Eq. (23) that the amplification factor  $Q$  is independent of  $A$ . But for the numerical result, with the increase of  $A$ , the maximum amplification factor  $Q$  decreases. The curve of the numerical simulation is away from the curve of the theoretical formulation which is similar to the underdamped system.

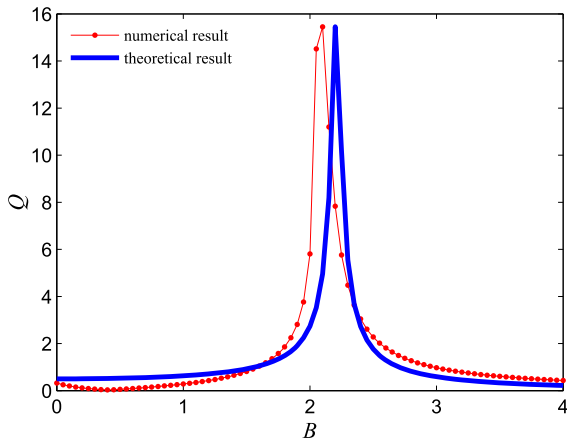


**Fig. 7** Amplification factor  $Q$  versus the amplitude of the HAS. The *thick line* is the theoretical result, while the *thin line with markers* is the numerical result. The simulation parameters are  $a = b = c = 10,000$ ,  $A = 0.01$ ,  $f = 100$  and  $F = 4000$

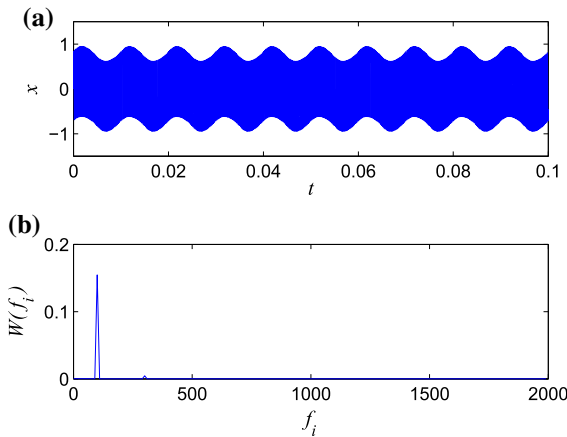


**Fig. 8** Output of the system when the VR occurs. **a** The time series of the output; **b** the amplitude spectrum of the response. The simulation parameters are  $a = b = c = 10,000$ ,  $A = 0.01$ ,  $B = 2.1$ ,  $f = 100$  and  $F = 4000$

In Fig. 10, the amplification factor  $Q$  versus the amplitude of the high-frequency auxiliary signal  $B$  is given for different value of  $f$ . With the increase of  $f$ , the amplification factor  $Q$  decreases. In this figure, it shows that the numerical and theoretical results are in close agreement, although the parameter  $f$  changes.

From Figs. 7, 8, 9 and 10, the VR is shown in the overdamped Duffing oscillator under different simulation parameters. When the VR occurs, the weak HCS can be detected.

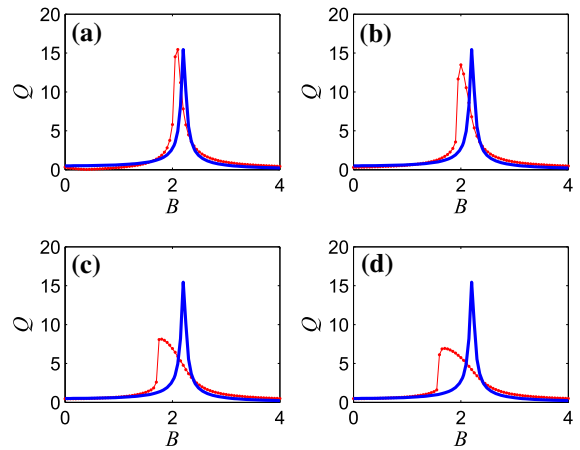


**Fig. 9** Amplification factor  $Q$  versus the amplitude of the HAS for **a**  $A = 0.01$ , **b**  $A = 0.03$ , **c**  $A = 0.09$ , **d**  $A = 0.12$ . The *thick lines* are the theoretical results, while the *thin lines with markers* are the numerical results. The simulation parameters are  $a = b = c = 10,000$ ,  $f = 100$  and  $F = 4000$

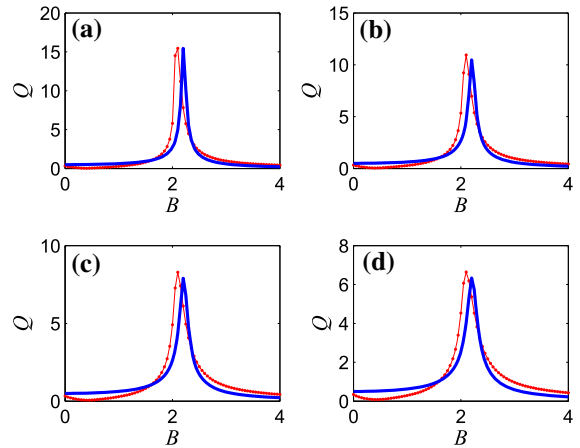


**Fig. 10** Amplification factor  $Q$  versus the amplitude of the HAS for **a**  $f = 100$ ; **b**  $f = 150$ ; **c**  $f = 200$ ; **d**  $f = 250$ . The *thick lines* are the theoretical results, while the *thin lines with markers* are the numerical results. The simulation parameters are  $a = b = c = 10,000$ ,  $A = 0.01$  and  $F = 4000$

#### 4 Conclusions

In order to detect the weak HCS, the scale transformation method which is used in SR is introduced in the investigation of the VR. We take the underdamped and the overdamped Duffing oscillators as examples, we carry out both the theoretical analysis and the numerical simulations. The theoretical results and the numerical results are in close agreement. Compared with the underdamped and overdamped Duffing oscillators, it

can be seen that the resonance pattern is different, but they also have some characteristics in common. Firstly, the curves of the theoretical results do not change with the increase in the amplitude of the weak HCS. Secondly, for the numerical results, with the increase in the amplitude of the weak HCS, the maximum amplification factor decreases. Finally, with the increase in the frequency of the weak HCS, the maximum amplification factor decreases in the numerical and the theoretical curves. It verifies that by introducing the scale transformation to the traditional VR theory, the weak HCS can be detected in an excellent manner. The method proposed in this paper can be applied to the detection of the weak high-frequency character signal. According to the method, we can determine the optimal design parameters of a detecting system. So, the method makes it possible to apply the theory of VR to deal with the engineering problems.

## References

- Landa, P.S., McClintock, P.V.E.: Vibrational resonance. *J. Phys. A Math. Gen.* **33**, 433–438 (2000)
- Benzi, R., Sutera, A., Vulpiani, A.: The mechanism of stochastic resonance. *J. Phys. A Math. Gen.* **14**, L453–L457 (1981)
- Gammaitoni, L., Hänggi, P., Jung, P., Marchesoni, F.: Stochastic resonance. *Rev. Mod. Phys.* **70**, 223–287 (1998)
- Anishchenko, V.S., Safonova, M.A., Chua, L.O.: Stochastic resonance in Chua's circuit. *Int. J. Bifurc. Chaos* **2**, 397–401 (1992)
- Duan, F., Chapeau-Blondeau, F., Abbott, D.: Double-maximum enhancement of signal-to-noise ratio gain via stochastic resonance and vibrational resonance. *Phys. Rev. E* **90**, 860–877 (2014)
- Chizhevsky, V.N., Giacomelli, G.: Experimental and theoretical study of the noise-induced gain degradation in vibrational resonance. *Phys. Rev. E* **70**, 062101 (2004)
- Chizhevsky, V.N., Giacomelli, G.: Improvement of signal-to-noise ratio in a bistable optical system Comparison between vibrational and stochastic resonance. *Phys. Rev. E* **71**, 011801(R) (2005)
- Chizhevsky, V.N., Giacomelli, G.: Experimental and theoretical study of vibrational resonance in a bistable system with asymmetry. *Phys. Rev. E* **73**, 022103 (2006)
- Deng, B., Wang, J., Wei, X.L., Tsang, K.M., Chan, W.L.: Vibrational resonance in neuron populations. *Chaos* **20**, 3–4 (2010)
- Sun, J.B., Deng, B., Liu, C., Yu, H.T., Wang, J., Wei, X.L., Zhao, J.: Vibrational resonance in neuron populations with hybrid synapses. *Appl. Math. Model.* **37**, 6311–6324 (2013)
- Yu, H.T., Guo, X.M., Wang, J., Deng, B., Wei, X.L.: Vibrational resonance in adaptive small-world neuronal networks with spike-timing-dependent plasticity. *Phys. A* **436**, 170–179 (2015)
- Yang, J.H.: Vibrational resonance in fractional-order anharmonic oscillators. *Chin. Phys. Lett.* **29**, 104501 (2012)
- Yang, J.H., Zhu, H.: Vibrational resonance in Duffing systems with fractional-order damping. *Chaos* **22**, 013112 (2012)
- Yang, J.H., Sanjuán Miguel, A.F., Tian, F., Yang, H.F.: Saddle-node bifurcation and vibrational resonance in a fractional system with an asymmetric bistable potential. *Int. J. Bifurcat. Chaos* **25**, 1550023 (2015)
- Wang, C.J., Yang, K.L.: Vibrational resonance in bistable gene transcriptional regulatory system. *Chin. J. Phys.* **50**, 607–618 (2012)
- Yang, L.J., Liu, W.H., Yi, M., Wang, C.J., Zhu, Q.M., Zhang, X., Jia, Y.: Vibrational resonance induced by transition of phase-locking modes in excitable systems. *Phys. Rev. E* **86**, 016209 (2012)
- Wang, C.J., Yang, K.L., Qu, S.X.: Vibrational resonance in a discrete neuronal model with time delay. *Int. J. Mod. Phys. B* **28**, 124–127 (2014)
- Jeevarathinam, C., Rajasekar, S., Sanjuán Miguel, A.F.: Vibrational resonance in groundwater-dependent plant ecosystems. *Ecol. Complex.* **15**, 33–42 (2013)
- Jeevarathinam, C., Rajasekar, S., Sanjuán Miguel, A.F.: Effect of multiple time-delay on vibrational resonance. *Chaos* **23**, 013136 (2013)
- Daza, A., Wagemakers, A., Rajasekar, S., Sanjuán Miguel, A.F.: Vibrational resonance in a time-delayed genetic toggle switch. *Commun. Nonlinear Sci. Numer. Simul.* **18**, 411–416 (2013)
- Coccolo, M., Litak, G., Seoane, J.M., Sanjuán Miguel, A.F.: Energy harvesting enhancement by vibrational resonance. *Int. J. Bifurc. Chaos* **24**, 1430019 (2014)
- Yang, J.H., Sanjuán Miguel, A.F., Liu, H.G.: Vibrational subharmonic and superharmonic resonances. *Commun. Nonlinear Sci. Numer. Simul.* **30**, 362–372 (2015)
- Balachandran, B., Magrab, E.B., Balachandran, A.P.: *Vibrations*. Cengage Learning, Melbourne (2008)
- Tan, J.Y., Chen, X.F., Wang, J.Y., Chen, H.X., Cao, H.R., Zi, Y.Y., He, Z.J.: Study of frequency-shifted and re-scaling stochastic resonance and its application to fault diagnosis. *Mech. Syst. Signal Process.* **23**, 811–822 (2009)
- Li, J.M., Chen, X.F., He, Z.J.: Multi-stable stochastic resonance and its application research on mechanical fault diagnosis. *J. Sound Vib.* **332**, 5999–6015 (2013)
- Lu, S.L., He, Q.B., Kong, F.R.: Effects of underdamped step-varying second-order stochastic resonance for weak signal detection. *Digit. Signal Process.* **36**, 93–103 (2015)
- He, Q.B., Wang, J., Liu, Y.B., Dai, D.Y., Kong, F.R.: Multi-scale noise tuning of stochastic resonance for enhanced fault diagnosis in rotating machines. *Mech. Syst. Signal Process.* **28**, 443–457 (2012)
- Thomsen, J.J.: *Vibrations and Stability: Advanced Theory, Analysis, and Tools*. Springer, Berlin (2003)
- Blekhman, I.I.: *Vibrational Mechanics: Nonlinear Dynamic Effects, General Approach. Applications*. World Scientific, Singapore (2000)
- Blekhman, I.I., Landa, P.S.: Conjugate resonances and bifurcations in nonlinear systems under biharmonic excitation. *Int. J. Nonlinear Mech.* **39**, 421–426 (2004)